



Published in final edited form as:

Calcif Tissue Int. 2010 November ; 87(5): 450–460. doi:10.1007/s00223-010-9404-x.

Contribution of mineral to bone structural behavior and tissue mechanical properties

Eve Donnelly^{1,*}, Dan X. Chen^{2,*}, Adele L. Boskey^{3,4,5}, Shefford P. Baker⁶, and Marjolein C. H. van der Meulen^{1,3}

¹Sibley School of Mechanical and Aerospace Engineering, Cornell University, Ithaca, NY

²Department of Biomedical Engineering, Cornell University, Ithaca, NY

³Musculoskeletal Integrity Program, Hospital for Special Surgery, New York, NY

⁴Department of Biochemistry, Weill Medical College of Cornell University, New York, NY

⁵Graduate Program in Physiology, Biophysics, and Systems Biology, Weill Medical College of Cornell University, New York, NY

⁶Department of Materials Science and Engineering, Cornell University, Ithaca, NY

Abstract

Bone geometry and tissue material properties jointly govern whole-bone structural behavior. While the role of geometry in structural behavior is well characterized, the contribution of the tissue material properties is less clear, partially due to the multiple tissue constituents and hierarchical levels at which these properties can be characterized. Our objective was to elucidate the contribution of the mineral phase to bone mechanical properties across multiple length scales, from the tissue material level to the structural level. Vitamin D and calcium deficiency in 6-week-old male rats was employed as a model of reduced mineral content with minimal collagen changes. The structural properties of the humeri were measured in three-point bending and related to the mineral content and geometry from microcomputed tomography. Whole-cortex and local bone tissue properties were examined with infrared (IR) spectroscopy, Raman spectroscopy, and nanoindentation, to understand the role of altered mineral content on the constituent material behavior. Structural stiffness (-47%) and strength (-50%) were reduced in vitamin D-deficient (-D) humeri relative to controls. Moment of inertia (-38%), tissue mineral density (TMD, -9%), periosteal mineralization (-28%), and IR mineral:matrix ratio (-19%) were reduced in -D cortices. Thus, both decreased tissue mineral content and changes in cortical geometry contributed to impaired skeletal load bearing function. In fact, 97% of the variability in humeral strength was explained by moment of inertia, TMD, and IR mineral:matrix ratio. The strong relationships between structural properties and cortical material composition demonstrate a critical role of the microscale material behavior in skeletal load-bearing performance.

Keywords

bone strength; material properties; mineral; rat; Fourier transform infrared spectroscopy

Corresponding author: Marjolein C. H. van der Meulen Sibley School of Mechanical and Aerospace Engineering Cornell University 219 Upson Hall Ithaca, NY 14853 Tel: (607) 255-1445 Fax: (607) 255-1222 mcv3@cornell.edu.

*These authors contributed equally to this study

Coauthors' email addresses: Eve Donnelly: donnellye@hss.edu Dan X. Chen: chend@hss.edu Adele L. Boskey: boskeya@hss.edu Shefford P. Baker: shefford.baker@cornell.edu

INTRODUCTION

Whole-bone structural behavior is governed by geometry and tissue material properties. The effect of geometry on structural properties is well understood [1], but the role of tissue material properties is less straightforward. Structural analyses of whole bones generally approximate effective material properties from the cross-sectional geometry and the measured structural properties by assuming that the tissue is homogeneous. However, bone tissue is a heterogeneous material with properties that vary both temporally and spatially within the tissue microstructure [2-6]. The values of tissue elastic modulus and ultimate stress estimated from whole-bone structural tests are considerably lower than would be expected based on nanoindentation results, and the effective material properties do not correlate with directly measured material properties [7,8]. Pathologic alterations in tissue composition also suggest an important role for material properties in bone fragility. Diseases such as osteoporosis not only reduce bone quantity but also alter tissue composition [4,9,10]. Changes in intra-specimen distributions of tissue material properties can substantially alter structural elastic and failure properties of bone tissue [11,12]. Therefore, spatial variations in tissue material properties play an important role in bone structural integrity.

Because material properties are determined by microstructure, changes in the primary microstructural constituents, collagen and mineral, are expected to change tissue properties. At the whole-bone level, bone mineral content plays a crucial role in bone structural behavior. The elastic modulus, yield stress, and ultimate stress of bone depend strongly on mineral content [13,14]. Similar relationships between mineral content and material properties must be established at the tissue level and related to whole-bone structural behavior.

The contributions of sub-micrometer-scale material parameters to bone structural behavior have been examined in several studies relating mineral properties [15] and nanomechanical properties [16,17] to structural properties of rat bones. Increased tissue mineral content, carbonate substitution, and crystallinity were associated with increased femoral bending stiffness, and inclusion of these parameters in addition to geometric properties in a multiple regression model improved the predictive power for structural behavior [15]. These investigations intriguingly point to modulation of bone structural behavior by changes in material properties arising from altered tissue composition. Comprehensive studies of structural, geometric, and material properties across multiple length scales are needed to characterize the contribution of tissue constituents to bone material and structural behavior.

In this investigation we focus on the role of mineral content in whole-bone behavior and tissue material properties. Well-established rodent dietary models provide a means to vary tissue composition in a controlled manner. Vitamin D deficiency in rats produces rickets and osteomalacia characterized by reduced bone mineral content and strength with minimal changes in collagen composition [18-21]. This model system allows isolation of the contribution of a single tissue constituent to structural and material properties, after accounting for changes in bone geometry. Our objective was to examine the contribution of mineral to bone tissue mechanical properties at multiple length scales using vitamin D deficiency as a model of reduced mineral content. We hypothesized that the changes in mechanical properties associated with reduced tissue mineral content would be similar across size scales, from macroscopic to sub-micrometer. In particular, bones with reduced tissue mineral content were hypothesized to be relatively weaker and more compliant on the structural level, as well as softer and more compliant on the tissue level.

MATERIALS AND METHODS

Study Design

Tissue of varying mineral content was investigated to elucidate the role of mineral in whole-bone structural behavior and bone tissue properties. A controlled reduction in bone tissue mineral content was achieved in growing rats through vitamin D deficiency [18,19,22]. The mechanical behavior and composition of Vitamin D-deficient and control humeri were assessed at the whole-bone and tissue levels. Whole-bone analyses comprising three-point bending, microcomputed tomography (microCT), and ashing were performed on the right humeri to characterize structural properties, architecture, and bone mineral content. Whole-cortex and local tissue-level analyses were performed on the left humeri to characterize tissue composition, mechanical properties, mineral crystal size, and collagen microstructure. The whole-cortex analyses assessed average cortical material properties using Fourier transform infrared (FTIR) spectroscopy and x-ray diffraction (XRD). The local analyses detailed tissue material properties in a selected sub-region of the cortex using nanoindentation, Raman spectroscopy, and second harmonic generation (SHG) microscopy.

Six-week-old male Sprague-Dawley rats were stratified by weight and alternately assigned to control or vitamin D-deficient (-D) groups. All animals were housed in the dark for the duration of the 4-week, IACUC-approved experiment. The -D group (n = 5) was fed a Ca- and vitamin D-deficient (0 IU/g D₃, 0.02% Ca, 0.2% P) diet [23], while the control group (n = 5) was paired a normal Ca- and vitamin D-replete diet (2 IU/g D₃, 0.53% Ca, 0.42% P). At the end of the experiment the body weights of the animals were similar across groups (-D 331 ± 27 g vs. Control: 337 ± 12 g, p = 0.65). Three animals per group were administered fluorochrome labels (IP, 15 mg/kg) 28, 14, and 4 days before euthanasia. Fluorescent labels interfere with SHG microscopy and were not administered to the remaining animals.

Histologic Analyses

Undecalcified distal ends of the radii and ulnae were embedded in poly(methyl methacrylate), and 6- μ m-thick longitudinal sections were stained with von Kossa and counterstained with neutral red. Images of the radial epiphyseal growth plates from a single section were digitally recorded at 4x magnification using two adjacent fields (1320 × 990 μ m²) that spanned the entire width of the growth plate. A region of interest comprising the entire growth plate, as well as a subregion of interest including only the hypertrophic zone, was drawn for each section, and the proximal-distal distances across each radial growth plate and hypertrophic zone were measured at 20 evenly spaced intervals (Bioquant Osteo, Nashville, TN).

For evaluation of cortical and trabecular osteoid fraction, images were recorded from one cortical field (1320 × 990 μ m²) of the most proximal end of the medial midshaft and one trabecular field (1320 × 990 μ m²) of the secondary trabeculae near the medial-lateral center line. The fraction of osteoid area in each image was calculated as osteoid area/(osteoid area + mineralized area) in each cortical and trabecular field (Bioquant Osteo, Nashville, TN).

Whole-bone Analyses

The structural behavior of the right humeri was assessed by 3-point bending to failure. The humeri were positioned on two supports 7.5 mm apart, with the deltoid tuberosity in the plane of bending. The central load was applied to the medial mid-diaphysis at 0.05 mm/s using a hydraulically actuated uniaxial load frame (Bionix 858, MTS Systems). Yield was defined as a 10% reduction in secant stiffness relative to the initial tangent stiffness [24]. The following parameters were calculated: bending stiffness (EI), failure moment (M_{fail}), displacements at yield (D_{yield}) and failure (D_{fail}), and post-yield displacement ($D_{fail} - D_{yield}$) [25,26].

The architecture and mineral content of the right humeri were characterized by microCT (MS-8, GE Healthcare). Inclusion of a calibration phantom allowed conversion of x-ray attenuation to mineral density [27]. Scans were reconstructed at 13.4- μm isotropic resolution. Global thresholds for whole-bone (0.185 g/cm^3), cortical (0.539 g/cm^3), and cancellous (0.185 g/cm^3) analyses were defined as the minimum specimen-specific threshold determined by the Otsu method [28] for each analysis type (MicroView, GE Healthcare).

Whole-bone composition was assessed with microCT followed by ashing. Whole-bone mineral content (BMC) and tissue mineral density (TMD = BMC/ bone volume (BV)) were obtained from microCT scans. Humerus length was defined as the distance between the most proximal and distal points. The humeri were ashed, and the ash fraction was calculated as ash weight/dry weight [29].

Cortical geometry and mineral content were quantified for a 3-mm-long mid-diaphyseal segment at the deltoid tuberosity. Cortical bone volume, BMC, and TMD were determined for the volume of interest. Cross-sectional properties, including cross-sectional area and moments of inertia were determined for each slice and averaged over the volume of interest. Moments of inertia in the medial-lateral and anterior-posterior planes (I_{ML} , I_{AP}) were calculated using the deltoid tuberosity as an anatomical marker of the anterior aspect of the humerus.

Mineral density distributions were measured across the posterior cortex of the mid-diaphysis, a region chosen to correspond to the areas examined with nanoindentation (see *Tissue-level Analyses*). Mineral density profiles were measured radially inward from the periosteal surface toward the endosteum. For each specimen, four single-voxel-wide profiles were averaged to give a single profile as a function of distance from the periosteal edge. The profiles for each specimen were then averaged to obtain a single mean mineral density profile for each group. The slope of each profile for the first $\sim 50 \mu\text{m}$ from the periosteal edge was calculated for each group.

Cancellous architecture and BMC were quantified from a total volume (TV) of $\sim 18 \text{ mm}^3$ (of cancellous bone) from the proximal epiphysis of each humerus. Trabecular thickness, trabecular separation, bone volume fraction (BV/TV), and TMD were determined for each group.

Tissue-level Analyses

Two sets of tissue-level analyses were performed on the left humeri: whole-cortex and local. The whole-cortex analyses assessed global changes in cortical material properties with impaired mineralization. The local analyses characterized in detail the spatial and temporal gradients in material properties in a subregion of the posterior cortex. The left humeri were sectioned at mid-diaphysis, and the proximal halves were designated for the whole-cortex analyses, while the distal halves were designated for the local analyses.

1. Whole-cortex Analyses—Mineral crystallite size in the c -axis dimension was assessed using XRD. Cortical diaphyseal segments taken from the proximal halves of the left humeri were lyophilized and ground to a fine powder. Diffraction patterns over the range $2\theta = 10^\circ$ - 40° were obtained using a powder diffractometer (Bruker AX8) with Ni-filtered Cu-K α incident radiation. The crystal thickness in the c -axis direction was estimated from the (002) peak width (FWHM) using the Scherrer formula [30]. FTIR spectra were then collected from KBr pellets prepared from the bone powders as described previously [31]. The spectra were analyzed for the mineral:matrix ratio, carbonate:phosphate ratio, collagen maturity, and mineral crystal size/perfection [31].

2. Local Analyses—Following dehydration and embedding, one 2-mm-thick transverse mid-diaphyseal section from each distal humerus was polished anhydrously [32]. Four regions of tissue in the posterior cortex, each $\sim 10 \mu\text{m} \times 1 \mu\text{m}$, were characterized with nanoindentation and Raman spectroscopy, as described previously [33], as well as SHG microscopy. These regions, demarcated by fluorochrome labels, corresponded to tissue ages of 0-4 d, 5-14 d, 15-28 d, and 29-70 d, with the youngest tissue at the periosteal surface. One analysis area in each of the four tissue age regions was identified on combined fluorescence and brightfield micrographs of each of the labeled specimens. Identification of fiducial features ensured that all local analyses were performed at the same locations.

The mechanical properties of the four analysis areas in each sample were characterized using nanoindentation. A scanning nanoindenter (TriboIndenter, Hysitron, Inc.) with a Berkovich diamond tip was used to image sample topography and collect force-displacement data. The tip was loaded into the sample at $50 \mu\text{N/s}$, held at a load of $500 \mu\text{N}$ for 10 s, and unloaded at $50 \mu\text{N/s}$, producing indentations with contact depths of $\sim 100 \text{ nm}$. The indentation modulus E and hardness H were calculated from the force-displacement data [34]. In each sample, four indentations spaced $3 \mu\text{m}$ apart were made near the center of each of the four analysis areas, along a line parallel to the periosteum. For the four specimens without fluorescent labels, for which tissue age boundaries could not be localized, boundary positions were estimated from the positions of the labels in the labeled specimens. The data collected from the unlabeled specimens were used only in the regressions with whole-bone measures to maximize the sample size (see *Statistical Analyses*).

The composition of the same tissue previously characterized by nanoindentation was assessed with Raman spectroscopy. Raman spectra over the range $800\text{-}1800 \text{ cm}^{-1}$ were collected using a Raman microprobe with a 785-nm laser (Renishaw, Inc.) and a $50\times$, 0.75 NA objective (Zeiss), producing a beam with a diameter of $\sim 1 \mu\text{m}$ at the specimen surface. For each sample, four spectra were collected near the center of each of the four regions within the cortex, along a line parallel to the periosteum. The spacing between the four spectrum collection points was $\sim 3 \mu\text{m}$. For each spectrum, three cosmic ray-corrected, 10-s exposures were acquired and averaged. Baseline corrections were made to all peaks before calculation of intensities of the phosphate ν_1 (959 cm^{-1}), carbonate ν_1 (1070 cm^{-1}), and amide I (1675 cm^{-1}) bands. The phosphate ν_1 and Amide I bands selected for Raman analysis are the most prominent vibrations for bone mineral and collagen, respectively, and are expected to have the greatest sensitivity in the characterization of hypomineralized tissue in vitamin D-deficient animals. While these bands may show some dependence on lamellar orientation [35], orientation effects are minimized in the woven bone tissue examined here. Intensity ratios of the phosphate/amide I bands and carbonate/phosphate bands were calculated to obtain the mineral:matrix ratio and the carbonate:phosphate ratio ($\text{CO}_3:\text{PO}_4$), respectively. As before, for the specimens without fluorescent labels, tissue age zones were estimated using the labeled samples to obtain data used only in the regression analyses.

To examine whether matrix changes were present with vitamin D deficiency, collagen organization was assessed using SHG microscopy [36]. This technique produces a spatial map of aligned collagen when a pulsed laser scanned within the sample generates a second harmonic signal upon interaction with collagen fibers [37,38]. Specimen dehydration is expected to affect the secondary structure of the collagen but not its orientation, and the highly oriented collagenous microstructure of lamellar bone is preserved in dehydrated specimens imaged with SHG microscopy [36]. The details of the SHG microscope have been described previously [36,37]. Briefly, incident light from a Ti:Sapphire laser (Spectra Physics) generating 100-fs pulses at 840 nm was focused on the sample with a $20\times$, 0.75 NA air objective (Zeiss). SHG light was collected in epifluorescent mode and optically filtered (BGG22) to remove backscattered incident light. The in-plane diameter (FWHM) of the focal volume was ~ 420

nm [38]. One 512×512 -pixel ($267 \times 267\text{-}\mu\text{m}^2$) image of each analysis region was collected for qualitative evaluation of collagen organization.

Statistical Analyses

The structural, geometric, and material properties were examined statistically to assess differences between the properties of the control and -D groups. Student's t-tests were performed on the structural parameters, the microCT-assessed cortical and cancellous geometric and mineral measures, the FTIR parameters, and the crystal dimensions. Repeated-measures ANOVAs with Fisher's PLSD post-hoc tests were performed on the mean E , H , and Raman mineral:matrix and $\text{CO}_3\text{:PO}_4$ values for each tissue age region. Linear regressions of pooled control and -D data were performed to examine relationships between mechanical, geometric, and compositional parameters within whole-bone and tissue levels. For the local tissue parameters, the material properties of the three oldest tissue age groups (5-14 d, 15-28 d, 29-70 d) were similar and, therefore, were averaged to obtain a single value for each animal for the regression analyses. Multiple regressions were used to evaluate the individual and combined effects of geometry and tissue material properties on structural behavior. A significance level of 0.05 was used for all analyses. Values are reported as mean \pm standard deviation.

RESULTS

Histologic Data

Histologic features confirming the presence of rickets and osteomalacia were observed in the distal radii of the vitamin D-deficient animals (Figure 1). The epiphyseal growth plates of the -D animals were 42% wider overall than those of the controls, due primarily to a widening of the hypertrophic zones (+55%). Prevalent osteoid was observed on the surfaces of trabecular and cortical bone in the -D animals (Figure 1). In the -D animals the area fraction of osteoid increased 453% and 256% in trabecular and cortical bone, respectively, relative to controls.

Whole-bone Data

In whole-bone bending tests, bending stiffness and failure moment were reduced 48% and 55%, respectively, in the -D group relative to controls (Table 1, Figure 2). Although no difference in total displacement to failure was observed, -D humeri exhibited larger post-yield displacement than the controls (+192 %).

The whole-bone compositional parameters obtained from microCT and ashing were consistently lower in the -D group (Table 2). Bone mineral content and tissue mineral density were reduced by 21% and 13% in the -D humeri relative to controls. The -D group had lower ash weight (-35%) and ash fraction (-7%) relative to the control group. Humerus length was not different between groups. As expected, whole-bone mineral content determined by microCT correlated with ash weight ($r^2 = 0.48$), and whole-bone mineral density correlated with ash fraction ($r^2 = 0.71$).

Vitamin D deficiency substantially reduced cortical cross-sectional area and moment of inertia (Table 2). Cortical bone volume (-34%), average cortical cross-sectional area (-36%), and average moments of inertia (-38% M-L, -40% A-P) were reduced in the -D humeri relative to controls. Increased endocortical porosity was evident in the -D humeri compared to the controls. Cortical bone mineral content and tissue mineral density were reduced by 39% and 9%, respectively, in the -D group relative to the control group. For both groups, tissue mineral density increased with distance from the periosteal edge for the first $\sim 50\ \mu\text{m}$ and remained constant thereafter. The initial mineral gradient of the -D group was reduced by 28% relative to that of the control group.

Vitamin D deficiency also altered cancellous architecture and tissue properties (Table 2). Trabecular thickness was reduced by 43% in the -D group relative to controls, and trabecular separation was not different between the two groups. The vitamin D-deficient humeri had a lower cancellous bone volume fraction (-24%) and tissue mineral density (-18%) than the controls. Cancellous tissue mineral density increased with bone volume fraction ($r^2 = 0.76$).

Tissue-level Data

1. Whole-Cortex Data—For the compositional properties obtained from FTIR spectroscopy, the mineral:matrix ratio was lower (-19%) in the -D group relative to the control group (4.34 ± 0.21 vs. 5.36 ± 0.39 , respectively). The carbonate:phosphate ratio (-D: 0.016 ± 0.0016 vs. Control: 0.018 ± 0.0020), collagen maturity (-D: 2.67 ± 1.60 vs. Control: 2.25 ± 1.12), and mineral crystal size/perfection (-D: 0.99 ± 0.01 vs. Control: 1.00 ± 0.01) were not different between groups. X-ray diffraction showed that crystallite *c*-axis length was not different between groups (-D: 10.3 ± 4.2 nm vs. Control: 10.9 ± 5.2 nm).

2. Local Data—In the subset of specimens characterized with nanoindentation, tissue indentation modulus and hardness increased rapidly and significantly with tissue age in both -D and control groups (Figure 3). The modulus of the newest periosteal tissue (0-4 d) was substantially lower than that of the older intracortical tissue (5-70 d). The moduli of the three older tissue age groups were similar. Despite the reduction in tissue modulus with vitamin D deficiency relative to controls at the middle time points (-12% at 5-14 d and -16% at 15-28 d), the overall effect of -D treatment was not significant. In the tissue that existed prior to the start of the experiment (29-70 d), the indentation modulus was similar for both -D and control groups. Parallel trends were observed for hardness, although the differences between treatment groups were less pronounced (Figure 3).

The variation in the local Raman compositional measures with tissue age was similar to that of the nanomechanical properties (Figure 3). The youngest tissue had the lowest mineral:matrix and $\text{CO}_3\text{:PO}_4$ ratios. The 5–14-day-old tissue had an intermediate mineral:matrix ratio, and the two oldest tissue age groups (15-70 d) had the greatest values. The $\text{CO}_3\text{:PO}_4$ ratios of the three oldest tissue age groups (5-70 d) were similar. Vitamin D deficiency reduced the mineral:matrix ratio of the 15–28-day-old tissue by 8% and the $\text{CO}_3\text{:PO}_4$ ratio of the 5-14 d and 15-28 d tissue by 5% and 9%, respectively, relative to controls, but these differences did not reach statistical significance ($p < 0.2$). In the tissue that existed prior to the start of the experiment (29-70 d), the mineral:matrix and $\text{CO}_3\text{:PO}_4$ ratios were similar for both groups.

Local tissue mechanical properties correlated with the local compositional measures. Statistical analysis of the regressions between each of the two nanomechanical and two Raman compositional measures revealed no differences in the slopes of the regression lines for control and -D groups; therefore, control and -D data were pooled. Tissue modulus increased with mineral:matrix ratio ($r^2=0.80$) (Figure 4) and with $\text{CO}_3\text{:PO}_4$ ratio ($r^2=0.82$). Similarly, hardness increased with mineral:matrix ratio ($r^2=0.75$) and with $\text{CO}_3\text{:PO}_4$ ratio ($r^2=0.76$).

The collagenous microstructures of control and -D tissue were qualitatively similar. SHG micrographs revealed relatively diffuse regions of aligned collagen characteristic of woven bone in the cortices of all specimens examined (data not shown).

Whole-bone and Tissue Property Correlations

When correlations between structural properties, geometry, and whole-cortex tissue properties were examined, bending stiffness and failure moment correlated strongly with the moment of inertia, TMD, and FTIR mineral:matrix ratio (Table 3). No other relationships between whole-bone and tissue properties were significant. When combined, geometric and tissue

compositional parameters from microCT (I_{AP} and TMD) explained 86% and 94% of the respective variations in bending stiffness and failure moment. When I_{AP} was combined with a different whole-cortex material metric, the FTIR mineral:matrix ratio, 88% and 94% of the respective variations in bending stiffness and failure moment were explained. These three measures (I_{AP} , TMD, and FTIR mineral:matrix ratio) combined to explain 97% of the variability in failure moment and 88% of the variation in bending stiffness, with both material metrics contributing independently to the failure moment, but not stiffness. Inclusion of the local nanomechanical properties and Raman compositional measures did not improve the predictive capability of the statistical model.

DISCUSSION

In the growing rat, Ca- and vitamin D deficiency reduced the extent of mineralization and appositional growth. Together, decreased appositional growth and tissue mineral content impaired skeletal load-bearing function, as evidenced by substantial reductions in bending stiffness (-48%) and strength (-55%). Furthermore, post-yield displacement nearly doubled in the -D group. These alterations in structural properties arose from changes in both cortical geometry and tissue material properties. Based on geometric changes alone, a 40% reduction in whole-bone strength and stiffness would be predicted; however, newly formed periosteal tissue with reduced stiffness and hardness, located far from the neutral axis of bending, would be expected to disproportionately reduce these structural properties. In addition to the altered cortical geometry, vitamin D deficiency induced tissue material changes, as evidenced by reductions in FTIR mineral:matrix ratio (-19%) and tissue mineral density (-9%). Humeri with reduced tissue mineral content were softer and more compliant at the local material level. Local tissue modulus was reduced ~15% in the 5–28-day-old tissue in the vitamin D-deficient group. Bone strength was best predicted by combining measures of tissue quantity, geometry, and material: cortical TMD, moment of inertia, and FTIR mineral:matrix ratio.

Local material properties were closely correlated with composition (Figure 4). Variation in local Raman mineral:matrix ratio explained 80% of the variation in indentation modulus. The relationships between Raman mineral:matrix ratio and indentation modulus were similar across treatment groups (-D vs. control) and across sites (humerus vs. femur [33]) (Figure 4). In addition, the youngest tissue (0-4 days) was softer, more compliant, and had lower Raman mineral:matrix and carbonate:phosphate ratios than older tissue (5-70 days) but attained the composition of the intracortical tissue within several days of formation (Figure 3), as observed previously in rat femoral cortices [33]. With vitamin D deficiency, moderate reductions (-15%) in these local tissue properties were evident at the intermediate tissue ages (5-28 d), but the overall effect of treatment on local mechanical properties and composition in the posterior cortex was not significant across all tissue ages. This result may reflect the small size of the subset of specimens (n=3/group) analyzed with nanoindentation and Raman spectroscopy because the whole-cortex FTIR mineral:matrix ratio (-19%) and tissue mineral density (-9%) were significantly reduced with vitamin D deficiency for the full set of specimens (n=5/group). Finally, the similarity of the -D and control cortices in SHG images indicated that vitamin D deficiency did not induce microstructural changes in the organic matrix.

Reduced bone strength, cross-sectional area, mineral content, and mineralization rate with vitamin D deficiency have been observed previously in separate studies examining whole-bone mechanical properties [20] and mineralization [18,19,39,40]. In mature rats vitamin D deficiency reduced femoral torsional strength by 20% and did not affect stiffness [20], changes more moderate than those observed here in growing animals. The observed 192% increase in postyield deformation in the -D rats parallels the 200% increase in ultimate displacement seen in vitamin D receptor null mice compared to their wild-type littermates [41]. Our 33% reduction in cortical cross-sectional area fell in the middle of the range of areal reductions observed in

vitamin D-deficient weanling rats fed diets with normal (-8%) and reduced (-50%) Ca levels [18,40]. When bone mineral content was examined, humeral ash fraction was 7% lower in vitamin D-deficient animals relative to controls, similar to a 14% reduction in ash fraction observed in vitamin D-deficient rat pups [42]. The 28% reduction in the spatial mineral gradient noted here was similar to a 27% reduction in temporal mineral apposition rate observed previously [18]. Local bone mineral content and material properties have not been examined previously in vitamin D-deficient animals.

When the contributions of bone geometry and tissue material properties to whole-bone mechanical behavior were examined, the strongest individual predictors of structural behavior were cortical moment of inertia, cortical TMD, and whole-cortex FTIR mineral:matrix ratio (r^2 0.49-0.86) (Table 4). Interestingly, the FTIR mineral:matrix ratio was a substantially better predictor of bending stiffness than TMD (r^2 0.70 vs. 0.49), explaining an additional 21% of the observed variation in structural stiffness. These are among the first reports of strong correlations between FTIR-assessed compositional measures and bone structural properties [43]. Multiple regressions combining geometric and material measures did not increase the explanatory power for bending stiffness. In contrast, multiple regressions combining moment of inertia, TMD, and whole-cortex FTIR mineral:matrix ratio substantially increased the explanatory power for failure moment (+11%) over the individual regressions, indicating these parameters contribute independently to bone strength. This combined regression maximized the predictive power for bone strength, explaining 97% of the observed variation. Therefore, bone strength was best predicted by a combination of measures of bone quantity, cross-sectional geometry, and whole-cortex tissue composition.

To predict whole-bone structural properties, global measures of tissue composition (TMD, FTIR mineral:matrix) had greater explanatory power than local tissue-level measures of material properties (Raman mineral:matrix, indentation modulus). Weak individual correlations between whole-bone structural properties and local tissue mechanical properties have been reported previously [8] and likely reflect the localized nature of the tissue-level measurements. The local tissue-level parameters were obtained from indentation tests of small, relatively homogeneous volumes in one quadrant of the cortex and do not capture spatial heterogeneity or the effects of material interfaces, defects, and porosity.

This investigation of the effect of mineral content on bone mechanical properties comprised analyses across multiple length scales, from the whole-bone level to the tissue level. Aspects of this problem have previously been examined separately without combining macroscopic and microscopic mechanical and compositional analyses [18-20,39,40]. A recent study examining mechanical properties at multiple length scales yielded insights into the mechanisms by which pharmaceutical treatments for osteoporosis alter fracture resistance [17]. Similarly, our approach enabled direct quantification of geometric and material contributions to structural performance, in contrast to estimation of effective material properties from whole-bone test data [1]. A consequence of this comprehensive approach was that the size of the subset of samples analyzed by nanoindentation and Raman spectroscopy ($n = 3/\text{group}$) may have been insufficient to detect local tissue-level differences between treatment groups. Relatively large differences would have been required to detect an overall effect of treatment because the RM-ANOVA examined the effect of treatment across all time points, and the tissue formed prior to the start of the experiment (29-70 days) was expected to be identical in both groups. Nevertheless, the number of samples that underwent whole-bone analyses ($n = 5/\text{group}$) is typical of investigations that directly quantify material and compositional properties [8,15,16] and was sufficient to detect differences in structural properties, bone geometry, tissue mineral density, and whole-cortex FTIR compositional measures. The repeated-measures study design allowed examination of changes in tissue properties within individual animals over time.

Alteration of a single tissue constituent, the bone mineral content, contributed to altered skeletal physiology and load-bearing performance. Preservation of the collagen microstructure with vitamin D deficiency indicated that the dietary intervention successfully modified only the mineral component of the tissue, as intended. A combination of geometric and material changes profoundly impaired structural function, reducing whole-bone strength and stiffness by a factor of two. Reduced bone mineral content also increased bone ductility. In the future, multiple experimental durations will help to clarify whether the observed changes in bone geometry are an adaptive response to altered tissue material properties, or whether changes in bone geometry and material properties occur concomitantly. Such investigations may elucidate the factors that contribute to skeletal fragility and help to improve therapies for skeletal pathologies.

Acknowledgments

We thank Dr. Stephen Doty and Jeanane Diouri for assistance with tissue processing and histology, Dr. Jacqueline Cole for assistance with mechanical testing and statistical analyses, Dr. Sylvia Christakos for advice on the study design, Hayat Taleb for x-ray diffraction and infrared spectroscopic analyses, and Dr. Junghyun Cho and Andy Zhang for help with nanoindentation. Funding was provided by the Cornell Center for Materials Research (NSF DMR 0520404), NIH (R01 AR053571, P30 AR046121), and the American Association of University Women Educational Foundation (Selected Professions Fellowship).

REFERENCES

1. van der Meulen MC, Jepsen KJ, Mikic B. Understanding bone strength: size isn't everything. *Bone* 2001;29:101–104. [PubMed: 11502469]
2. Boivin GY, Chavassieux PM, Santora AC, Yates J, Meunier PJ. Alendronate increases bone strength by increasing the mean degree of mineralization of bone tissue in osteoporotic women. *Bone* 2000;27:687–694. [PubMed: 11062357]
3. Nuzzo S, Peyrin F, Cloetens P, Baruchel J, Boivin G. Quantification of the degree of mineralization of bone in three dimensions using synchrotron radiation microtomography. *Med Phys* 2002;29:2672–2681. [PubMed: 12462734]
4. Paschalis EP, Betts F, DiCarlo E, Mendelsohn R, Boskey AL. FTIR microspectroscopic analysis of human iliac crest biopsies from untreated osteoporotic bone. *Calcified Tissue International* 1997;61:487–492. [PubMed: 9383276]
5. Paschalis EP, Betts F, DiCarlo E, Mendelsohn R, Boskey AL. FTIR microspectroscopic analysis of normal human cortical and trabecular bone. *Calcif Tissue Int* 1997;61:480–486. [PubMed: 9383275]
6. Paschalis EP, DiCarlo E, Betts F, Sherman P, Mendelsohn R, Boskey AL. FTIR microspectroscopic analysis of human osteonal bone. *Calcif Tissue Int* 1996;59:480–487. [PubMed: 8939775]
7. Jepsen KJ, Schaffler MB, Kuhn JL, Goulet RW, Bonadio J, Goldstein SA. Type I collagen mutation alters the strength and fatigue behavior of Mov13 cortical tissue. *J Biomech* 1997;30:1141–1147. [PubMed: 9456382]
8. Silva MJ, Brodt MD, Fan Z, Rho JY. Nanoindentation and whole-bone bending estimates of material properties in bones from the senescence accelerated mouse SAMP6. *J Biomech* 2004;37:1639–1646. [PubMed: 15388305]
9. Boskey A, Mendelsohn R. Infrared analysis of bone in health and disease. *J Biomed Opt* 2005;10:031102. [PubMed: 16229627]
10. Faibish D, Ott SM, Boskey AL. Mineral changes in osteoporosis: a review. *Clin Orthop Relat Res* 2006;443:28–38. [PubMed: 16462423]
11. Bourne BC, van der Meulen MC. Finite element models predict cancellous apparent modulus when tissue modulus is scaled from specimen CT-attenuation. *J Biomech* 2004;37:613–621. [PubMed: 15046990]
12. Jaasma MJ, Bayraktar HH, Niebur GL, Keaveny TM. Biomechanical effects of intraspecimen variations in tissue modulus for trabecular bone. *J Biomech* 2002;35:237–246. [PubMed: 11784542]
13. Currey JD. The effect of porosity and mineral content on the Young's modulus of elasticity of compact bone. *J Biomech* 1988;21:131–139. [PubMed: 3350827]

14. Burstein AH, Zika JM, Heiple KG, Klein L. Contribution of collagen and mineral to the elastic-plastic properties of bone. *J Bone Joint Surg Am* 1975;57:956–961. [PubMed: 1184645]
15. Akkus O, Adar F, Schaffler MB. Age-related changes in physicochemical properties of mineral crystals are related to impaired mechanical function of cortical bone. *Bone* 2004;34:443–453. [PubMed: 15003792]
16. Hengsberger S, Ammann P, Legros B, Rizzoli R, Zysset P. Intrinsic bone tissue properties in adult rat vertebrae: modulation by dietary protein. *Bone* 2005;36:134–141. [PubMed: 15664011]
17. Brennan TC, Rizzoli R, Ammann P. Selective modification of bone quality by PTH, pamidronate, or raloxifene. *J Bone Miner Res* 2009;24:800–808. [PubMed: 19063681]
18. Baylink D, Stauffer M, Wergedal J, Rich C. Formation, mineralization, and resorption of bone in vitamin D-deficient rats. *J Clin Invest* 1970;49:1122–1134. [PubMed: 5422016]
19. Donnelly R, Bockman R, DiCarlo E, Betts F, Boskey A. The effect of gallium nitrate on healing of vitamin D- and phosphate-deficient rickets in the immature rat. *Calcif Tissue Int* 1993;53:400–410. [PubMed: 8293354]
20. Einhorn TA, Bonnarens F, Burstein AH. The contributions of dietary protein and mineral to the healing of experimental fractures. A biomechanical study. *J Bone Joint Surg Am* 1986;68:1389–1395. [PubMed: 3782211]
21. Bielaczyc AR, Golebiewska M, Citko A, Rogowski F. Concentration of the cross-linked carboxyterminal telopeptide of type I collagen in serum of young growing rats fed a low calcium and vitamin D-deficient diet. *Eur J Clin Chem Clin Biochem* 1997;35:915–918. [PubMed: 9476619]
22. Kaastad TS, Reikeras O, Halvorsen V, Falch JA, Obrant KJ, Nordsletten L. Vitamin D deficiency and ovariectomy reduced the strength of the femoral neck in rats. *Calcif Tissue Int* 2001;69:102–108. [PubMed: 11683422]
23. Pansini AR, Christakos S. Vitamin D-dependent calcium-binding protein in rat kidney. Purification and physicochemical and immunological characterization. *J Biol Chem* 1984;259:9735–9741. [PubMed: 6430904]
24. Jepsen KJ, Goldstein SA, Kuhn JL, Schaffler MB, Bonadio J. Type-I collagen mutation compromises the post-yield behavior of Mov13 long bone. *J Orthop Res* 1996;14:493–499. [PubMed: 8676263]
25. Torzilli PA, Takebe K, Burstein AH, Heiple KG. Structural properties of immature canine bone. *J Biomech Eng* 1981;103:232–238. [PubMed: 7311488]
26. Young, WC. *Roark's Formulas for Stress and Strain*. McGraw-Hill; New York: 1989.
27. Fritton JC, Myers ER, Wright TM, van der Meulen MC. Loading induces site-specific increases in mineral content assessed by microcomputed tomography of the mouse tibia. *Bone* 2005;36:1030–1038. [PubMed: 15878316]
28. Otsu N. A threshold selection method from gray-level histograms. *IEEE Transactions on Systems, Man, and Cybernetics SMC* 1979;9:62–66.
29. Carter DR, Caler WE, Spengler DM, Frankel VH. Fatigue behavior of adult cortical bone: the influence of mean strain and strain range. *Acta Orthop Scand* 1981;52:481–490. [PubMed: 7331784]
30. Cullity, BD.; Stock, SR. *Elements of X-Ray Diffraction*. Prentice-Hall; Upper Saddle River, NJ: 2001.
31. Faibish D, Gomes A, Boivin G, Binderman I, Boskey A. Infrared imaging of calcified tissue in bone biopsies from adults with osteomalacia. *Bone* 2005;36:6–12. [PubMed: 15663997]
32. Donnelly E, Baker SP, Boskey AL, van der Meulen MCH. Effects of surface roughness and maximum load on the mechanical properties of cancellous bone measured by nanoindentation. *Journal of Biomedical Materials Research* 2006;77A:426–435. [PubMed: 16392128]
33. Donnelly E, Boskey AL, Baker SP, van der Meulen MC. Effects of tissue age on bone tissue material composition and nanomechanical properties in the rat cortex. *J Biomed Mater Res A* 2010;92:1048–1056. [PubMed: 19301272]
34. Oliver WC, Pharr GM. Improved technique for determining hardness and elastic modulus using load and displacement sensing indentation experiments. *Journal of Materials Research* 1992;7:1564–1583.
35. Kazanci M, Wagner HD, Manjubala NI, Gupta HS, Paschalis E, Roschger P, Fratzl P. Raman imaging of two orthogonal planes within cortical bone. *Bone* 2007;41:456–461. [PubMed: 17602910]

36. Donnelly E, Williams RM, Downs SA, Dickinson ME, Baker SP, van der Meulen MCH. Quasistatic and dynamic nanomechanical properties of cancellous bone tissue relate to collagen content and organization. *Journal of Materials Research* 2006;21:2106–2117.
37. Williams RM, Zipfel WR, Webb WW. Interpreting second-harmonic generation images of collagen I fibrils. *Biophysical Journal* 2005;88:1377–1386. [PubMed: 15533922]
38. Zipfel WR, Williams RM, Webb WW. Nonlinear magic: multiphoton microscopy in the biosciences. *Nature Biotechnology* 2003;21:1369–1377.
39. Weinstein RS, Underwood JL, Hutson MS, DeLuca HF. Bone histomorphometry in vitamin D-deficient rats infused with calcium and phosphorus. *Am J Physiol* 1984;246:E499–505. [PubMed: 6377910]
40. Stauffer M, Baylink D, Wergedal J, Rich C. Decreased bone formation, mineralization, and enhanced resorption in calcium-deficient rats. *Am J Physiol* 1973;225:269–276. [PubMed: 4722387]
41. Amling M, Priemel M, Holzmann T, Chapin K, Rueger JM, Baron R, Demay MB. Rescue of the skeletal phenotype of vitamin D receptor-ablated mice in the setting of normal mineral ion homeostasis: formal histomorphometric and biomechanical analyses. *Endocrinology* 1999;140:4982–4987. [PubMed: 10537122]
42. Brommage R, DeLuca HF. Vitamin D-deficient rats produce reduced quantities of a nutritionally adequate milk. *Am J Physiol* 1984;246:E221–226. [PubMed: 6703051]
43. Weinstein RS, Wan C, Liu Q, Wang Y, Almeida M, O'Brien CA, Thostenson J, Roberson PK, Boskey AL, Clemens TL, Manolagas SC. Endogenous glucocorticoids decrease skeletal angiogenesis, vascularity, hydration, and strength in aged mice. *Aging Cell* 2010;9:147–161. [PubMed: 20047574]

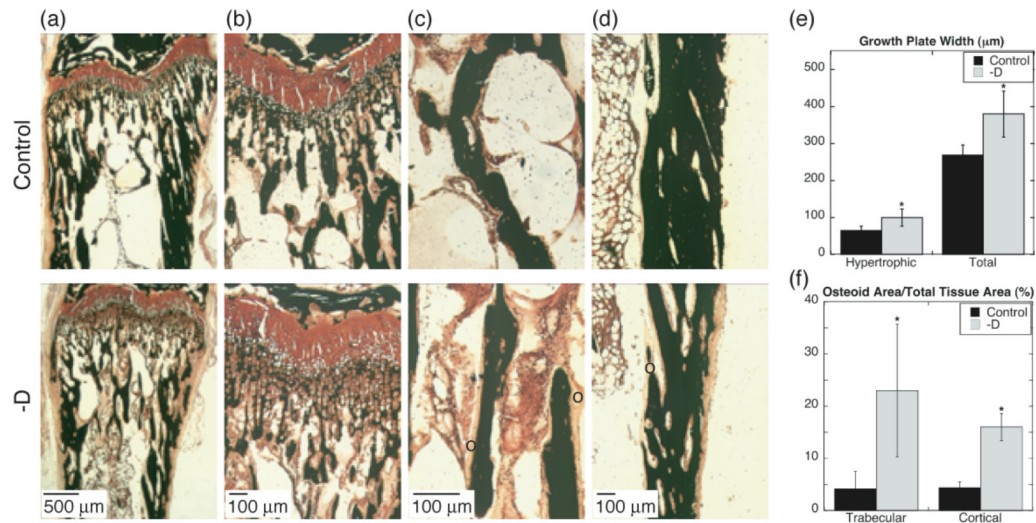


Figure 1. Histology of distal radii of 10-week-old control and vitamin D-deficient (-D) rats. Von Kossa stain with neutral red counterstain of (a) distal radii, (b) growth plates, (c) trabecular bone, and (d) cortical bone (o = osteoid). Cartilage, osteoid, and bone appear red, light pink, and black, respectively. (e) Growth plate hypertrophic zone and total widths. (f) Percent osteoid area for trabecular bone and cortical bone (* $p < 0.05$ vs. control).

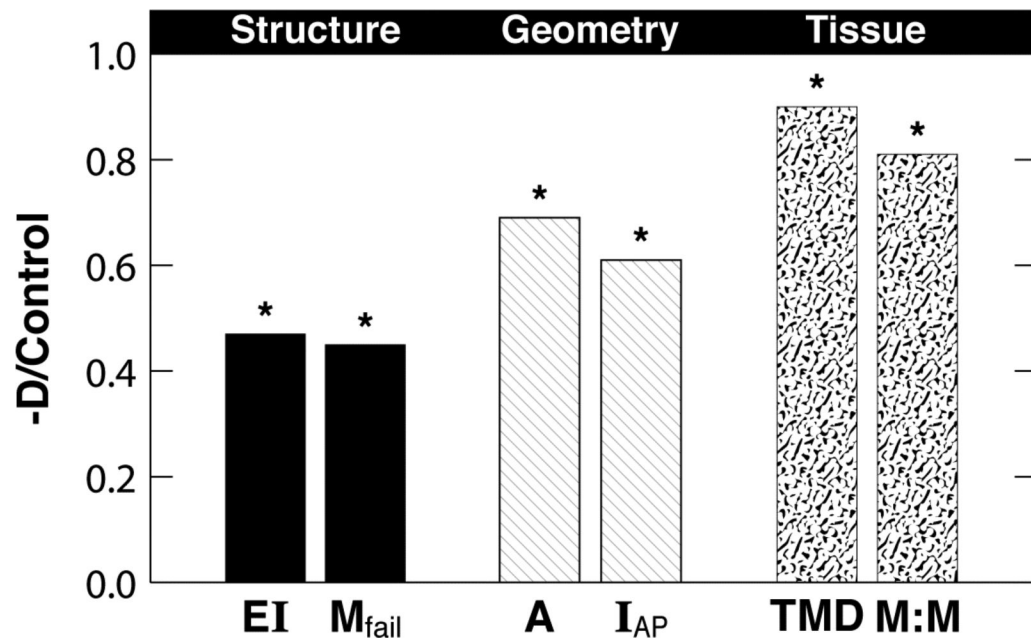


Figure 2. Mean structural, geometric, and tissue mineral measures of the vitamin D-deficient (-D) group normalized by the control values. (EI = bending stiffness, M_{fail} = failure moment, A = cortical area, I_{AP} = anterior-posterior moment of inertia, TMD = tissue mineral density, and M:M = FTIR mineral:matrix ratio.) * indicates $p < 0.05$ -D vs. control by t-test.

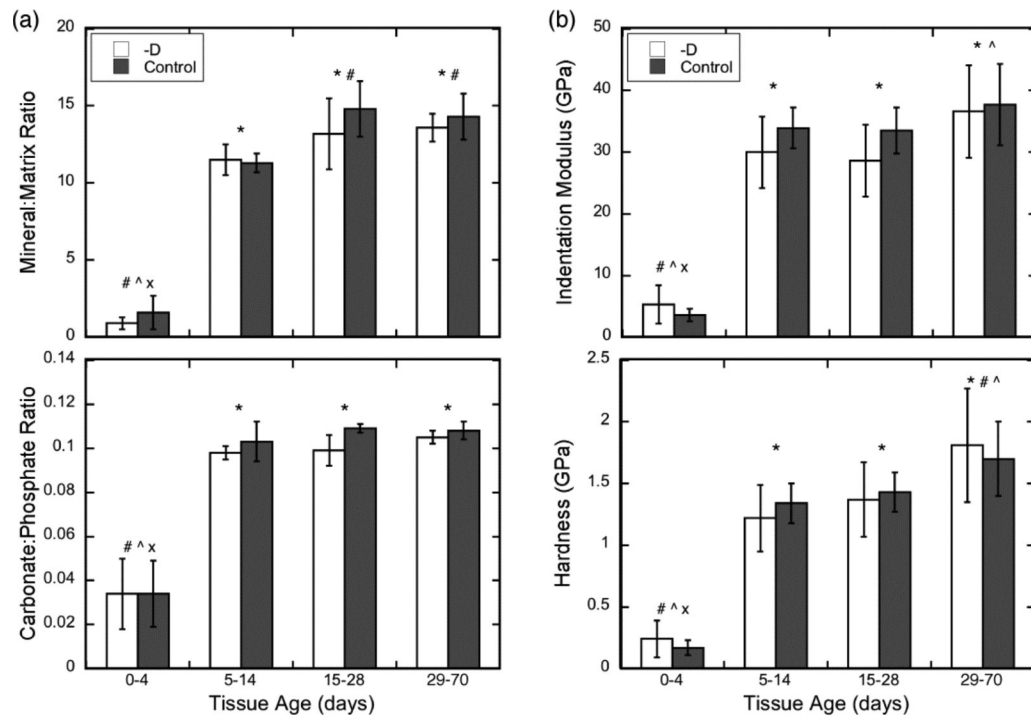


Figure 3. Local tissue (a) compositional and (b) nanomechanical properties. Error bars depict standard deviations. (* p < 0.05 vs. 0-4 days, # p < 0.05 vs. 5-14 days, ^ p < 0.05 vs. 15-28 days, x p < 0.05 vs. 29-70 days by RM-ANOVA)

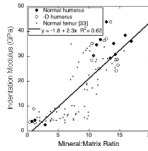


Figure 4. Regression analyses of tissue indentation modulus vs. mineral:matrix ratio for humeri analyzed in the current study (circles, mean values, $r^2 = 0.80$) and femora analyzed previously (squares, individual measurements, $r^2 = 0.54$) [33].

Table 1

Whole-bone properties from three-point bending, microCT, and ashing; mean (SD).

Variable	Control	Vitamin D-Deficient	Difference vs. Control
Length (mm)	27.8 (0.5)	28.2 (0.3)	+1%
Bending stiffness (N-mm ²)	2590 (260)	1340 (180)*	-48%
Failure moment (N-mm)	262 (18)	112 (12)*	-57%
Failure displacement (mm)	0.64 (0.05)	0.69 (0.07)	+8%
Post-yield displacement (mm)	0.09 (0.09)	0.27 (0.07)*	+192%
Whole-bone mineral content (mg)	232 (25)	184 (32)*	-21%
Whole-bone tissue mineral density (mg/mm ³)	0.43 (0.01)	0.38 (0.01)*	-13%
Ash weight (mg)	143 (5)	94 (3)*	-35%
Ash fraction	0.67 (0.01)	0.62 (0.02)*	-7%

*
(p < 0.05) vs. control

Table 2

Cortical and cancellous architecture and mineral measures; mean (SD).

Variable	Control	Vitamin D-Deficient	Difference vs. Control
Cortical bone volume (mm ³)	11 (0.4)	7.2 (0.3)*	-34%
Cross sectional area (mm ²)	3.6 (0.1)	2.3 (0.1)*	-36%
Moment of inertia _{ML} (mm ⁴)	1.9 (0.2)	1.2 (0.1)*	-38%
Moment of inertia _{AP} (mm ⁴)	2.0 (0.1)	1.2 (0.1)*	-40%
Cortical bone mineral content (mg)	12 (0.6)	7.2 (0.4)*	-39%
Cortical tissue mineral density (mg/mm ³)	1.1 (0.04)	1.0 (0.02)*	-9%
Cortical mineral gradient (mg/mm)	13 (2)	9 (2)*	-28%
Trabecular thickness (μm)	45 (5)	25 (4)*	-43%
Trabecular separation (μm)	21 (3)	22 (7)	5%
Cancellous bone volume fraction	0.66 (0.05)	0.50 (0.08)*	-24%
Cancellous tissue mineral density (mg/mm ³)	0.49 (0.02)	0.40 (0.02)*	-18%

* (p < 0.05) vs. control

Table 3

Coefficient of variation (r^2) for single and multiple regressions of selected geometric and material properties with bending stiffness and failure moment.

Geometric or Material Parameters	Bending Stiffness (N-mm²)	Failure Moment (N-mm)
Cortical I _{AP}	0.86*	0.86*
Cortical TMD	0.49*	0.76*
FTIR Mineral:Matrix	0.70*	0.83*
Cortical I _{AP} + Cortical TMD	0.86*	0.94*
Cortical I _{AP} + FTIR Mineral:Matrix	0.88*	0.94*
Cortical I _{AP} + Cortical TMD + FTIR Mineral:Matrix	0.88*	0.97*

I_{AP} = anterior-posterior moment of inertia, TMD = tissue mineral density, and FTIR = Fourier transform infrared

* indicates $p < 0.05$.